

Structure of a turbulent boundary layer studied by DNS

Philipp Schlatter, Qiang Li, Geert Brethouwer,
Arne V. Johansson, Dan S. Henningson

1 Introduction and numerical method

Turbulent boundary layers constitute one of the basic building blocks for understanding turbulence, particularly relevant for industrial applications. Although the geometries in technical but also geophysical applications are complicated and usually feature curved surfaces, the flow case of a canonical boundary layer developing on a flat surface has emerged as an important setup for studying wall turbulence, both via experimental and numerical studies. However, only recently spatially developing turbulent boundary layers have become accessible via direct numerical simulations (DNS). The difficulties of such setups are mainly related to the specification of proper inflow conditions, the triggering of turbulence and a careful control of the free-stream pressure gradient. In addition, the numerical cost of such spatial simulations is high due to the long, wide and high domains necessary for the full development of all relevant turbulent scales. We consider a canonical turbulent boundary layer under zero-pressure-gradient via large-scale DNS. The boundary layer is allowed to develop and grow in space. The inflow is a laminar Blasius boundary layer, in which laminar-turbulent transition is triggered by a random volume force shortly downstream of the inflow. This trip force, similar to a disturbance strip in an experiment [7, 8], is located at a low Reynolds number to allow the flow to develop over a long distance. The simulation covers thus a long, wide and high domain starting at $Re_\theta = 180$ extending up to the (numerically high) value of $Re_\theta = 4300$, based on momentum thickness θ and free-stream velocity U_∞ . Fully turbulent flow is obtained from $Re_\theta \approx 500$. The numerical resolution for the fully spectral numerical method [2] is in the wall-parallel directions $\Delta x^+ = 9$ and $\Delta z^+ = 4$, resolving the relevant scales of motion. The simulation domain requires a total of $8 \cdot 10^9$ grid points in physical space, and was thus run massively parallel with 4096 processors.

Philipp Schlatter *et al.*,
Linné FLOW Centre, KTH Mechanics, Stockholm, Sweden, and
Swedish e-Science Reserach Centre (SeRC), e-mail: pschlatt@mech.kth.se

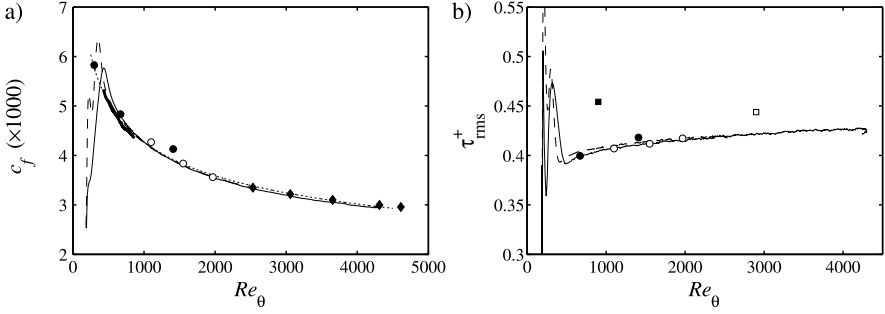


Fig. 1 Skin-friction coefficient c_f and wall-shear-stress fluctuations τ_{rms}^+ : solid: present DNS [7], dashed: DNS Schlatter *et al.* [8], dotted: $c_f = 0.024Re_\theta^{-0.25}$, thick solid: DNS Li *et al.* [5]. • DNS Spalart [10], ◦: DNS Simens *et al.* [9], ◻: DNS Ferrante and Elghobashi [3], ◼: DNS Wu and Moin [11], and ◈: experiments Österlund [6].

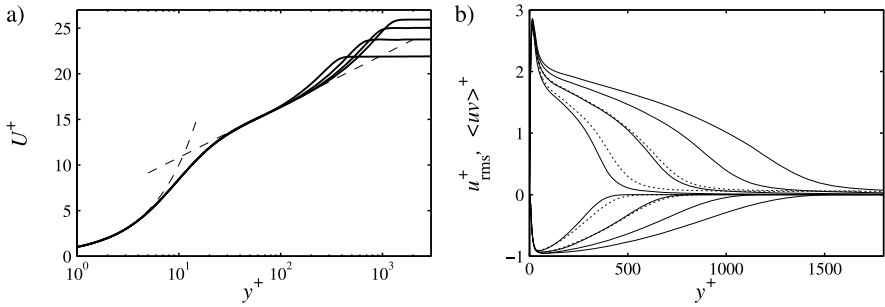


Fig. 2 Mean velocity profile U^+ , streamwise fluctuations u_{rms}^+ and shear stress $\langle uv \rangle^+$ at four $Re_\theta = 1100, 2000, 3000$ and 4100 ; solid: present DNS, dotted: DNS by Simens *et al.* [9]. dashed: log law with $\kappa = 0.41$ and $B = 5.2$.

2 Results

2.1 Turbulent statistics and streamwise development

Turbulence statistics obtained in the boundary layer such as mean profiles, fluctuations, two-point correlations *etc.* of the flow are in good agreement with other simulations, see also Refs. [7, 8], and experimental studies at similar Reynolds numbers [6]. To illustrate, Fig. 1 shows the skin-friction coefficient c_f and the fluctuating wall-shear stress τ_{rms} , compared to literature data. It turns out that the skin friction can be well described using the simple relation $c_f = 0.024Re_\theta^{-0.25}$ for the present Re_θ -range. In particular $\tau_{rms}^+ = u'/U|_{y \rightarrow 0}$ appears to be a sensitive measure for the development of the near-wall turbulence [7]. Mean velocity and stress profiles are shown in Fig. 2, compared to the DNS by Simens *et al.* [9]; the comparison to experiments at the higher Re is not shown here due to space restrictions (see however the comparisons provided *e.g.* in Ref. [8]).

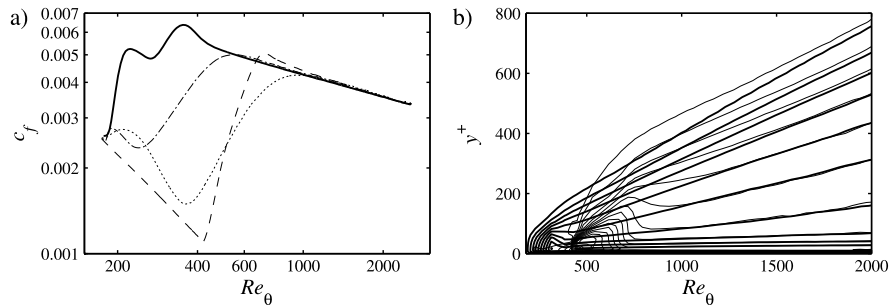


Fig. 3 a) Skin-friction coefficient c_f for various trippings: solid: “baseline” case, dot-dashed: lower amplitude and dotted: lower frequency trippings, dashed: classical transition via exponential growth of TS waves. b) Contours of u_{rms}^+ (spacing 0.25) for baseline case (thick) and TS-wave case (thin lines).

It is striking to see differences in the fluctuations profiles at $Re_\theta = 1100$ between our DNS and Ref. [9], which seem to have greatly reduced at $Re_\theta = 2000$. To further study the dependence of the boundary layer on initial conditions (*i.e.* the way how turbulence is induced), a series of DNS with varying tripping parameters has been performed. Fig. 3a) shows c_f for these DNS: Depending on tripping, laminar-turbulent transition is induced at different Re_θ , but the curves quickly settle on a common $c_f(Re_\theta)$ distribution, indicating a rather quick adaptation of the near-wall turbulence. Note also the typical overshoots of c_f as a result of transition. On the other hand, as shown in Fig. 3b), the outer-layer convergence, illustrated by contours of u_{rms} takes considerably longer than near the wall. Precisely this effect causes the discrepancies shown in Fig. 2b). It is worth noting that the profiles of the TS-wave-tripped DNS closely match the rms-profiles of Ref. [9] in Fig. 2. It remains an open question what conditions to apply for a “fully-developed” state of the boundary layer, and, consequently, whether a generic boundary layer at such low Re_θ exists.

When it comes to spectral information recorded in the boundary layer (not shown), spatial structures of two very distinct spatial (and temporal) scales are detected, *i.e.* the well-known turbulent streaks close to the wall scaling in inner (viscous) units, and long and wide structures scaling in outer units. These large-scale structures persist throughout the boundary layer from the free stream down to the wall and act as a modulation of the near-wall streaks. It is thus clear that the interplay of these two structures, scaling in different way, is strongly dependent on the Reynolds number, *i.e.* the downstream distance.

2.2 Vortical coherent structures

However, the characteristics of these large-scale structures, and their relation to actual coherent structures present in the flow are not entirely clear, in particular for higher Reynolds numbers. Recent studies, summarized by Adrian [1] and also ob-

served in a DNS of low- Re boundary layers [11] suggest a dominance of hairpin-shaped vortices of various sizes throughout the boundary layer. Hairpins are well-known structures in transitional flows, *e.g.* appearing as the results of shear-layer roll-up. It is now interesting to see whether hairpin-like structures persist in fully turbulent flow (either in the outer region or close to the wall), or whether they are mainly restricted to low- Re or transitional flows. Thus, we would like to study the structural characteristics of a turbulent boundary layer as a function of Reynolds number, starting from the transitional phase up to fully turbulent flow at higher Re than available in previous studies.

Figures 4 to 7 included here show small sections of the large simulation domain, each of them only visualising about 5% of the length of the full simulation domain. Each figure highlights different development stages of the boundary layer. Isocontours of negative λ_2 [4] identifying vortical structures are colored by the wall distance. Laminar-turbulent transition (Fig. 4) is induced by a trip forcing as described above. The subsequent breakdown to turbulent flow is characterized by the appearance of velocity streaks and unambiguous hairpin vortices, which are seen to dominate the whole span of the flow, see *e.g.* Ref. [1]. The hairpin vortices increase in number, and individual distinctive heads of such vortices are clearly visible for some distance downstream (Fig. 5 at $Re_\theta = 600$). This feature of low- Re turbulent flow is also put forward in Ref. [11], there denoted as “forest of hairpins”. We can thus confirm that, at least at low- Re , hairpins are indeed the dominant structure in a turbulent boundary layer. However, as the Reynolds number is further increased above about 1000, the scale separation between inner and outer units is getting larger, and the flow is less and less dominated by these transitional flow structures. At $Re_\theta = 2500$, as shown in Fig. 6, isolated instances of arches belonging to hairpin vortices can still be observed riding on top of the emerging outer-layer streaky structures. But the dominance of hairpin-like structures is clearly lower than in the previous figures closer to transition. This effect is even increased by considering the highest present Reynolds number, $Re_\theta = 4300$ as shown in Fig. 7. Then, individual hairpins or arches cannot be seen any longer. The boundary layer now is truly turbulent, and the outer layer is dominated by large-scale streaky organization of the turbulent vortices. Ongoing analysis of the flow structures close to the wall (*i.e.* the near-wall cycle) reveals characteristic oscillations of the near-wall streak, mainly in a sinuous manner leading to a staggered appearance of the vortex cores.

3 Summary and conclusions

A large DNS of a turbulent boundary layer has been performed reaching up to $Re_\theta = 4300$. The statistics are in very good agreement with available experimental measurement. The focus of the present contribution is twofold: First, an assessment of the importance of initial conditions at low Re_θ , and secondly, an analysis of coherent structure at higher Re_θ . It is for instance shown that various turbulence statistics can be significantly influenced up to $Re_\theta \approx 2000$ by the choice of tripping

Fig. 4 Visualization of the structures in a turbulent boundary layer by isocontours of negative λ_2 [4]; color code represents wall distance. The middle of the visualized domain is located at about $Re_\theta = 400$. Transition to turbulence can be observed by the appearance of Λ and hairpin vortices. No individual turbulent spots can be seen as the breakdown is happening simultaneously along the span.

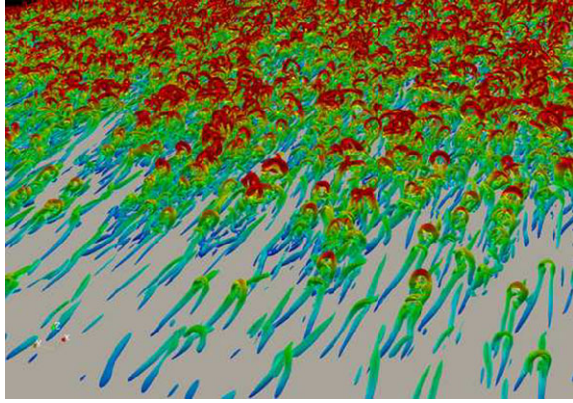


Fig. 5 Visualization of the structures in a turbulent boundary layer at about $Re_\theta = 600$. The whole span of the flow is clearly turbulent, *i.e.* dominated by random, unsteady vortical motion. However, the dominance of hairpin vortices as a remainder of transition are still the dominating coherent structures. Note that there is no clear scale separation yet given the low Re_θ .

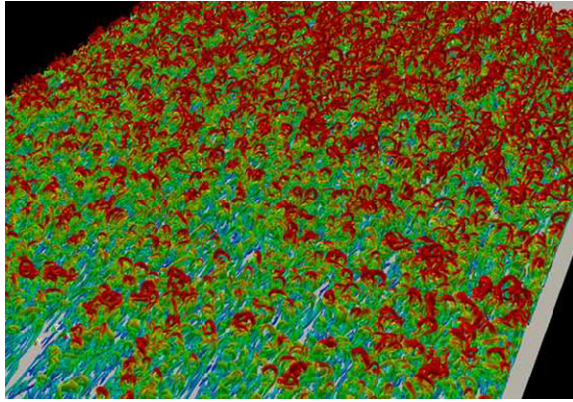
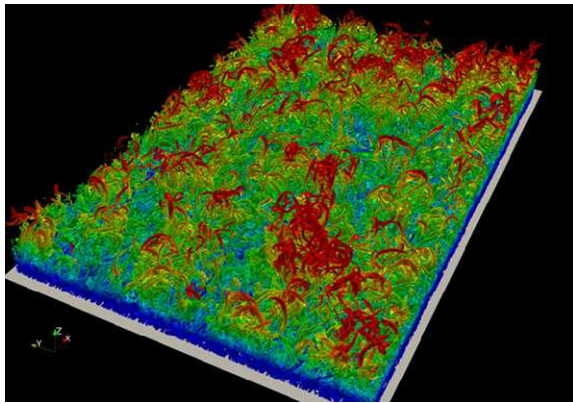
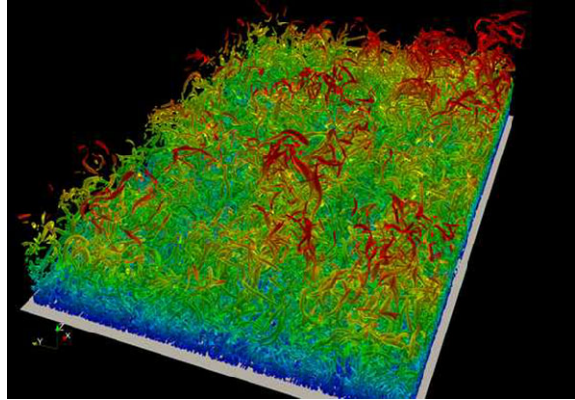


Fig. 6 Visualization of the structures in a turbulent boundary layer at about $Re_\theta = 2500$. The visualized domain has a length of about 7000 and a width of about 4500 viscous units. The intermittent structures close to the boundary-layer edge are clearly visible; they even arrange in large-scale bulges. The vortices do not span the whole boundary-layer height; the near-wall region is characterized by its own dynamics.



position and type; these differences relate to the behavior of the flow in the outer region of the boundary layer. Whether a generic boundary layer exists at such low Reynolds numbers clearly deserves more in-depth analysis. In a second part, the

Fig. 7 Visualization of the structures in a turbulent boundary layer at about $Re_\theta = 4300$. As in the previous frame, large-scale corrugation of the boundary-layer edge can be seen. The regular hairpin vortices seen close to transition have completely disappeared and are replaced by much more chaotic structures. Note also that the typical eddy diameter is practically unchanged compared to the previous figure.



coherent structures in the outer layer are studied. It is clearly shown that hairpin vortices, being characteristic transitional remainders at lower Reynolds numbers, are not visible any longer for higher Re .

Simulation data: www.mech.kth.se/~pschlatt/DATA

Acknowledgements Computer time was provided by the Swedish National Infrastructure for Computing (SNIC) with a generous grant by the Knut and Alice Wallenberg Foundation (KAW).

References

1. R. J. Adrian. Hairpin vortex organization in wall turbulence. *Phys. Fluids*, 19(041301):1–16, 2007.
2. M. Chevalier, P. Schlatter, A. Lundbladh, and D. S. Henningson. SIMSON - A Pseudo-Spectral Solver for Incompressible Boundary Layer Flows. Technical Report TRITA-MEK 2007:07, KTH Mechanics, Stockholm, Sweden, 2007.
3. A. Ferrante and S. Elghobashi. Reynolds number effect on drag reduction in a microbubble-laden spatially developing turbulent boundary layer. *J. Fluid Mech.*, 543:93–106, 2005.
4. J. Jeong and F. Hussain. On the identification of a vortex. *J. Fluid Mech.*, 285:69–94, 1995.
5. Q. Li, P. Schlatter, L. Brandt, and D. S. Henningson. DNS of a spatially developing turbulent boundary layer with passive scalar transport. *Int. J. Heat Fluid Flow*, 30:916–929, 2009.
6. J. M. Österlund. *Experimental studies of zero pressure-gradient turbulent boundary-layer flow*. PhD thesis, Department of Mechanics, KTH Stockholm, Sweden, 1999.
7. P. Schlatter and R. Örlü. Assessment of direct numerical simulation data of turbulent boundary layers. *J. Fluid Mech.*, 659:116–126, 2010.
8. P. Schlatter, R. Örlü, Q. Li, G. Brethouwer, J. H. M. Fransson, A. V. Johansson, P. H. Alfredsson, and D. S. Henningson. Turbulent boundary layers up to $Re_\theta = 2500$ studied through numerical simulation and experiments. *Phys. Fluids*, 21(051702):1–4, 2009.
9. M. P. Simens, J. Jiménez, S. Hoyas, and Y. Mizuno. A high-resolution code for turbulent boundary layers. *J. Comput. Phys.*, 228:4218–4231, 2009.
10. P. R. Spalart. Direct simulation of a turbulent boundary layer up to $Re_\theta = 1410$. *J. Fluid Mech.*, 187:61–98, 1988.
11. X. Wu and P. Moin. Direct numerical simulation of turbulence in a nominally zero-pressure-gradient flat-plate boundary layer. *J. Fluid Mech.*, 630:5–41, 2009.



<http://www.springer.com/978-94-007-2481-5>

Direct and Large-Eddy Simulation VIII

Kuerten, H.; Geurts, B.; Armenio, V.; Fröhlich, J. (Eds.)

2011, XII, 456 p., Hardcover

ISBN: 978-94-007-2481-5